27

Jupiter's Inner Radiation Belts

Scott J. Bolton
Jet Propulsion Laboratory, California Institute of Technology

Richard M. Thorne
Dept. of Atmospheric Sciences, University of California, Los Angeles

Sebastien Bourdarie
Office National d'Etudes et de Recherches Aerospatiales, Toulouse

Imke DePater
Dept. of Astronomy, University of California, Berkeley

Barry Mauk
The Johns Hopkins University Applied Physics Laboratory

27.1 HISTORICAL INTRODUCTION

The radiation belts of both Earth and Jupiter were discovered nearly simultaneously during the late 1950s. In the terrestrial case, the discovery of radiation belts followed the launch of *Explorer 1* in 1958 (Van Allen 1959). The equivalent radiation belts at Jupiter were serendipitously discovered after the detection of bursts of jovian radio emission in the decametric wavelength band by Burke and Franklin in 1955. Following the decametric detection, radio observations of Jupiter became more frequent, and by 1958 observations at a few centimeters measured a black body disk temperature of approximately 150 K, indicative of the temperature of Jupiter's atmosphere near 1 bar. In 1958, emission at 10.3 cm wavelength measured a temperature of >650 K (Sloanaker 1959, McClain and Sloanaker 1959), suggesting a non-thermal component, and attention quickly focused to developing potential explanations for the non-thermal radiation. By 1959 a number of plausible decimetric radiation mechanisms had been proposed, including synchrotron emission from a jovian radiation belt (Field 1959, Drake and Hvatum 1959). The determination that the jovian synchrotron emission was linearly polarized (Radhakrishnan and Roberts 1960) left no doubt that Jupiter was surrounded by a trapped radiation belt of energetic electrons. Studies of the similarities between the two known magnetospheres began shortly thereafter, and by the early 1960s, the field of comparative magnetospheres was effectively born.

Since their discovery, the inner (<5 R_J) jovian radiation belts have been routinely monitored by radio telescope observations. Occasional in situ measurements have also been obtained from spacecraft traveling directly through the belts. As interest in planetary exploration developed over the last few decades, the need to send spacecraft to explore Jupiter drove a special interest in the jovian radiation belts. Jupiter's inner radiation belts were soon recognized as one of the most hazardous regions in the solar system. Detailed knowledge of the energetic particle environment is needed for design of radiation tolerant spacecraft for future exploration of the jovian system.

The radiation belts of a planet form in the portion of the magnetosphere containing closed field lines. At Jupiter this region extends out radially to 50–100 R_J (Figure 27.1). It is convenient to subdivide the jovian magnetosphere into three regions. In the outer magnetosphere (>20–30 R_J), the breakdown of corotation (Hill 1979) leads to intense field-aligned currents (e.g., Bunce and Cowley 2001), which have been linked to jovian auroral emissivity. The middle magnetosphere (5–30 R_J) contains the four Galilean moons, among which Io provides the major source of plasma for the entire system. The inner magnetosphere (<5 R_J) is a region of strong magnetic field and low plasma density inside of the Io torus (Figure 27.1). This region includes Jupiter's innermost satellites (Metis, Adrastea, Amalthea, Thebe), the main, halo and gossamer ring systems, and the region where Jupiter's magnetic field is in synchronous rotation with Keplerian orbital motion (~2.24 R_J, analogous to geosynchronous orbit at Earth). The structure of the high-energy radiation belts, which form in this region, is the topic of this chapter. The reader is referred to the other chapters for discussions of the middle and outer magnetosphere.

Our current understanding of Jupiter's inner radiation belts has been developed from a combination of synchrotron observations, in situ measurements from a small handful of spacecraft, and theoretical considerations based on our knowledge of Jupiter's system and comparison with the terrestrial radiation belts. We now have a more complete picture of the major effects responsible for the differences be-

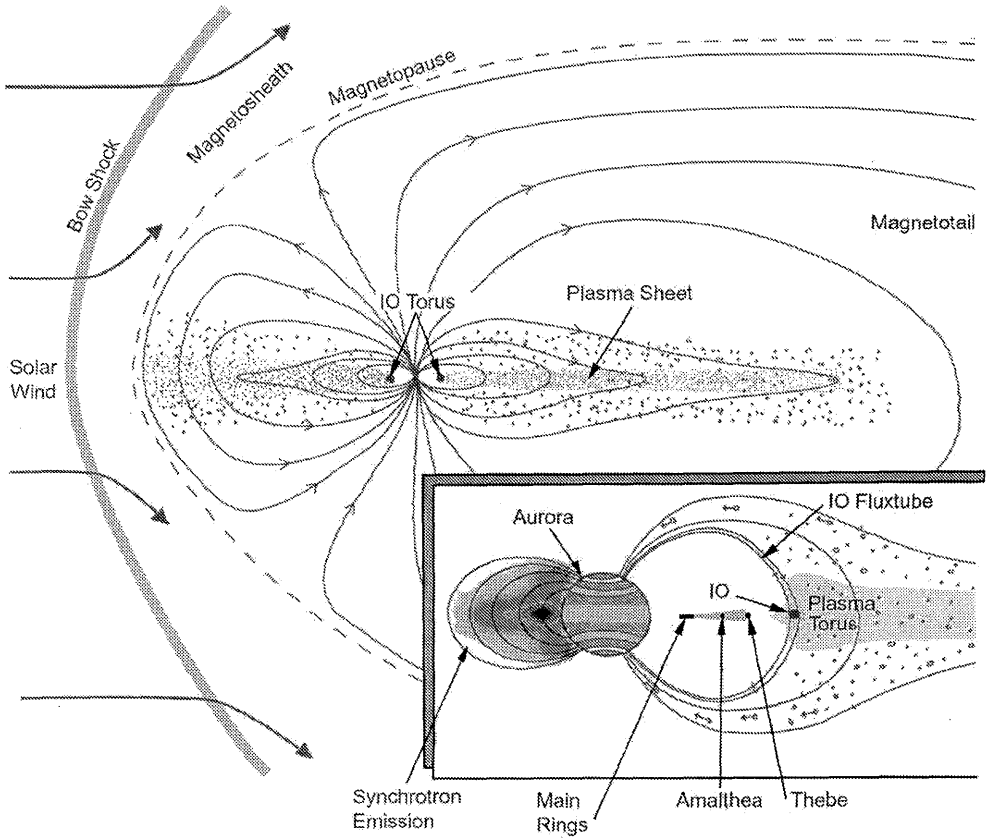

Figure 27.1. Sketch of Jupiter's magnetosphere illustrating the relationship between the inner, middle and outer magnetospheric regions. Inset shows the primary components of the inner radiation belts as discussed in this chapter. (Figure scale is approximate. From F. Bagenal, private communication.)

tween Jupiter's and Earth's radiation belts. The distribution of high-energy particles has been modified by interactions with Jupiter's ring system, inner moons, and extended atmosphere. The harshness of the environment requires considerable effort and advanced technology to prepare the radiation shielded spacecraft necessary to successfully carry out exploration of Jupiter's system. Only four spacecraft have probed the inner radiation belts to provide direct in situ measurements of the system. In 1973, *Pioneer 10* made a near-equatorial approach in to 2.85 R_J; in 1974, *Pioneer 11* made a high-inclination pass in to 1.6 R_J; in 1995, the *Galileo* probe made a near-equatorial penetration to the surface; and most recently, in 2002, the *Galileo* orbiter spacecraft carried out a close flyby of Jupiter's moon Amalthea ($\sim$2.54 R_J). In 2003, the *Galileo* orbiter made a final pass through the radiation belts en route to its "end of mission" collision with Jupiter's atmosphere.

In this chapter we will review the knowledge of Jupiter's inner radiation belts ($L < 5$) and the contributions made by the in situ measurements of *Pioneer*, *Galileo* probe and orbiter, and the decimetric radio observations of Jupiter's synchrotron emission. In the following sections, we describe the basic measurements and relate results from analyzing the data to advances in theoretical models. We discuss the physical processes that control the inner jovian radiation belts and the potential for future exploration of this hazardous radiation environment.

27.2 PHYSICAL PROCESSES IN JUPITER'S INNER RADIATION BELTS

27.2.1 Overview

Observations of energetic particles in the radiation belts of both the Earth and Jupiter generally exhibit a phase space density profile with a positive radial gradient (e.g., Ye and Armstrong 1993). Radial diffusion, in which the third adiabatic invariant is violated (while effectively conserving the first two invariants), may thus provide a potential source for the inner radiation zone in each magnetosphere. For the case of Earth, Lyons and Thorne (1973) were able to explain the observed two-zone structure of the electron belts as a simple balance between inward radial diffusion and scattering loss to the atmosphere. No internal sources are required to account for the quiet-time structure of the inner belt and the slot region between the inner and outer radiation belts. Particles are energized during the inward diffusion, as long as the first invariant is approximately conserved. At Jupiter energetic electrons responsible for the broad spectrum of synchrotron emission near $L = 1.5$ (where $B = 1$ G) require kinetic energies in the range $E_k = 5$–50 MeV. Direct in situ measurements over this energy range are incomplete, so remote sensing by synchrotron radiation is an invaluable tool. The first invariant of such highly relativistic electrons, $\mu = p^2/2mB = (E_k/B)(1 + E_k/2E_0)$, where $E_0 = mc^2$ is the rest energy, spans the range 30–2500 MeV/G. If such

electrons are provided by inward radial diffusion, the kinetic energy of the source population would be 700 keV–7 MeV near the orbit of Io (where $B \sim 2000$ nT), or 100 keV–2 MeV near the orbit of Europa (where $B \sim 400$ nT). Properties of these source electrons were directly measured in the middle jovian magnetosphere by instruments on the *Voyager* spacecraft (Krimigis *et al.* 1981), and more recently by *Galileo* (Williams *et al.* 1999, Mauk *et al.* 1999). Such satellite data can thus be used as an outer boundary condition for computational models of the inner jovian environment, even though the origin of relativistic electrons in the middle magnetosphere remains unresolved. During the inward transport, the electrons are subject to various processes, such as interactions with the small inner moons, interactions with the rings, energy loss by synchrotron radiation, and scattering loss to the atmosphere of Jupiter (e.g., Santos-Costa *et al.* 2001, Santos-Costa and Bourdarie 2001). The principal processes important to developing accurate models of the belts are briefly described below and in section 27.6.

27.2.2 Radial Diffusion

In the Earth's magnetosphere, radial diffusion is driven by fluctuating ultra-low frequency (ULF) waves or substorm-induced convection electric fields. The radial transport can be described by diffusion coefficients which scale as $D_{LL} = D_0\ L^n$, typically with $6 < n < 10$ (Schulz and Lanzerotti 1974) and a scaling coefficient D_0, which increases with the level of geomagnetic activity (Brautigam and Albert 2000). Due to the large size of the jovian magnetosphere, and the slow azimuthal drift rate of energetic particles, the processes that dominate at Earth are ineffective in the inner magnetosphere of Jupiter. Instead, radial diffusion in the inner jovian magnetosphere is assumed to be driven by ionospheric dynamo winds, as first suggested by Brice and McDonough (1973). The form of the diffusion coefficient then scales as $D_{LL} = D_0 L^3$, with typical diffusion times to the heart of the synchrotron zone comparable to a year (Coroniti 1974, Bolton *et al.* 1989, de Pater and Goertz 1990). A number of authors have analyzed the radial flux decreases associated with satellite absorption to estimate the radial diffusion coefficient. By using a simple absorption model both Simpson and McKibben (1976) and Mogro-Campero *et al.* (1975) obtained radial diffusion coefficients comparable to $D_{LL} = 10^{-10} L^4\ s^{-1}$, which agrees favorably with theoretical estimates by Brice and McDonough (1973), Birmingham *et al.* (1974), and Coroniti (1975).

27.2.3 Wave–Particle Interactions

Whistler-mode wave particle interactions (e.g., Dungey 1963, Cornwall 1964, Lyons *et al.* 1972) and Coulomb scattering (Walt and McDonald 1964) provide the dominant electron loss process in the inner magnetosphere of Earth (Abel and Thorne 1998), and thus control the radial structure of the inner radiation belt and slot region. At Jupiter, while wave scattering is an important process in the outer and middle magnetosphere (Thorne 1983), a recent analysis of *Galileo* PWS data from the Amalthea flyby indicates that whistler-mode waves are suppressed in the inner jovian magnetosphere (Gurnett, private communication 2003). This is probably due to the high magnetic field and low plasma density present inside the Io torus. Although one cannot rule out the possibility of wave induced scattering, the modeling by Santos-Costa and Bourdarie (2001) provide an acceptable fit to *Pioneer* observations of the inner zone of Jupiter, without the inclusion of wave scattering.

27.2.4 Sweeping Effect of the Jovian Moons

Four small jovian moons (Metis ($L = 1.79$), Adrastea ($L = 1.80$), Amalthea ($L = 2.54$), and Thebe ($L = 3.10$)) can contribute to the loss of energetic electrons (Mogro-Campero 1976, de Pater 1981, Santos-Costa and Bourdarie 2001) during inward radial diffusion from a source population in the middle magnetosphere. It is generally assumed that all particles colliding with any moon are absorbed. However, if the moon is magnetized or highly conducting, magnetic perturbations can deflect energetic particles (Thorne *et al.* 1999) and thus prevent a collision. Sweeping loss rates are sensitive to the electron energy which controls the azimuthal magnetic gradient drift rate, and to pitch angle, due to the inclination of Jupiter's magnetic equator to the spin equator, where the moons orbit (Figure 27.2). Particles with magnetic mirror points above or below the moon orbital plane (pitch angles $110° > \alpha > 70°$) have a much smaller probability of suffering a collision, leading to a strong pancake shaped distribution (peaked at $\alpha = \pi/2$) inside the orbits of the moons. This results in the strong confinement of synchrotron emission inside the orbit of Amalthea (the largest of these moons) to a region close to the equatorial plane.

27.2.5 Interaction with the Rings

Energetic electrons can also be absorbed as they pass through the thin jovian rings ($1.3 < L < 3.10$), which are usually assumed to be composed of dust with typical size between 0.1–100 μm (Showalter *et al.* 1987, Ockert-Bell *et al.* 1999). Because much larger dust particles are required to cause significant absorption at highly relativistic energies, the overall loss rate due to the rings is less important than that due to the moons. However, their effect still needs to be included and it gives rise to a noticeable absorption signature that was observed by the *Pioneer 11* spacecraft (Fillius 1976) and *Galileo* probe (Fischer *et al.* 1996). The main ring and halo extend from 1.25 R_J to 1.81 R_J and are approximately 10^2 and 10^4 km thick, respectively. In this region the optical depth is approximately 3×10^{-6} (see Chapter 11). The gossamer ring makes up the outer portion of the ring system and extends from 1.81 R_J to 3.10 R_J. As described in Chapter 11, the gossamer ring properties experience a step evolution at 2.54 R_J, the orbit of Amalthea, and again at 3.10 R_J, the orbit of Thebe. The thickness grows from 3×10^3 km to 6×10^3 km near the boundary of Thebe's orbit. Presumably, the ring particles are bound by the satellites with the thickness of the rings being correlated with the inclination of the satellite's orbit (Thebe is more inclined than Amalthea).

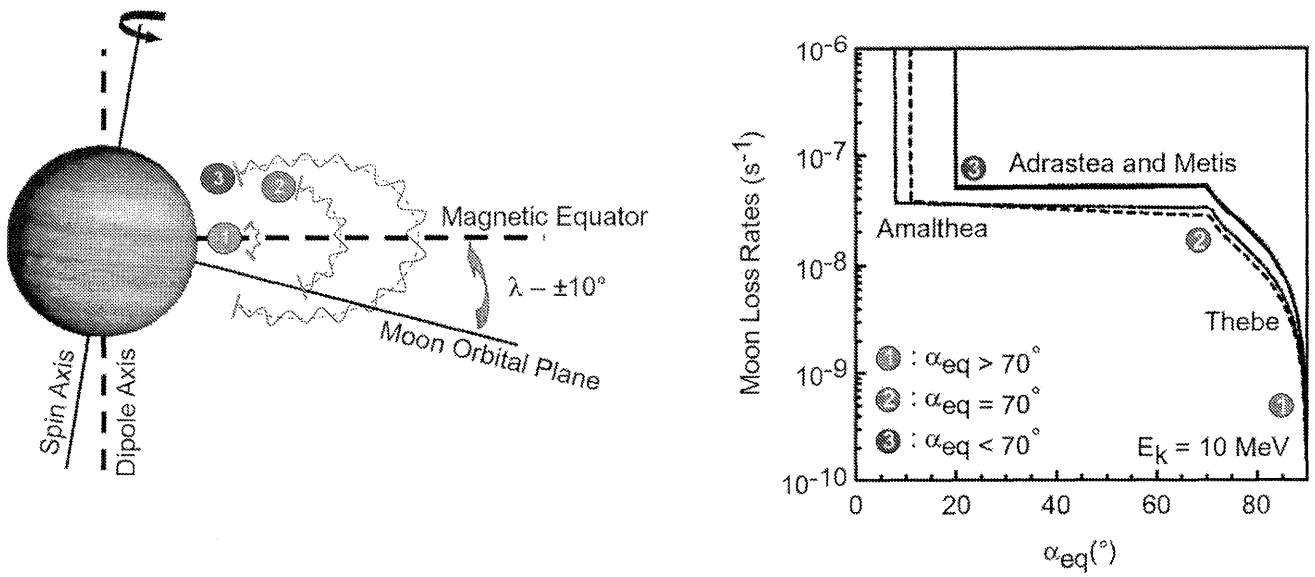

Figure 27.2. Illustration depicting the dependence of satellite sweeping on particle pitch angle. Due to the tilt of Jupiter's magnetic field with respect to Jupiter's rotational equator, and the inclination of the satellites' orbital planes, an electron with pitch angle greater than 70° has a greater chance of diffusing past the satellites without being lost as compared to an electron of the same energy with pitch angle less than 70°. From Santos-Costa (2001).

27.2.6 Synchrotron Radiation Loss

Synchrotron radiation causes relativistic electron energy degradation (in the direction perpendicular to the ambient magnetic field) and consequently a decrease in the trapped electron pitch angle. This drives the mirror point of relativistic electrons towards higher latitude and ultimately causes loss due to collision with the jovian atmosphere. The effective lifetime associated with synchrotron emission is inversely proportional to the ambient magnetic field strength and the square of the electron energy. Synchrotron emission is thought to become the dominant loss mechanism in the high field region ($L < \sim 1.8$), and this likely leads to the sharp inner edge in the synchrotron radiation pattern near 1.4 R_J.

27.2.7 Loss to the Atmosphere

Electrons that make it into the inner portion of the synchrotron zone are ultimately removed due to collisions in the jovian atmosphere (Abel and Thorne 2003). Because of strong magnetic anomalies associated with higher order moments in the internal jovian field (Acuna and Ness 1976), the electron drift trajectories are not at constant altitude. All particles that are transported into the region inside 1.3 R_J follow drift trajectories that eventually collide with the dense atmosphere (e.g., Wang *et al.* 2002). This loss is expected to be responsible for the steep drop in electron flux seen by the *Galileo* probe (Fischer *et al.* 1996).

27.2.8 Summary of Relevant Timescales

Relativistic electrons near the heart of the synchrotron zone gyrate rapidly ($\tau_{gyr} < 10^{-4}$ s) around the field and execute bounce motion between magnetic mirror points on timescales comparable to a few seconds. In addition to their corotation with the magnetic field structure, the electrons also experience westward azimuthal magnetic gradient drift with timescales comparable to a few days (de Pater 1981, Leblanc *et al.* 1997a). These basic adiabatic motion timescales are several orders of magnitude shorter than the non-adiabatic timescales associated with inward radial diffusion (years to reach $L = 1.5$ from the middle magnetosphere) or loss due to collisions with the moons or the rings and the emission of synchrotron radiation (Santos-Costa and Bourdarie 2001). Consequently, it is unlikely that significant azimuthal variation can be maintained in the inner radiation zone, since any gradients would rapidly be smeared out by the adiabatic motion. Temporary azimuthal structure was observed during the SL–9 impacts with Jupiter (Sault *et al.* 1997).

27.3 IN SITU OBSERVATIONS

The first in situ measurements of the jovian inner radiation belts were made by *Pioneer 10* and *11*, which carried a broad spectrum of energetic particle detectors (Table 27.1). Subsequently, measurements by the *Galileo* probe and more recently by the *Galileo* orbiter were more limited in their energy or spatial coverage, but provided important contributions to our understanding of the processes and distribution of high-energy particles in the belts. The *Pioneer 10* and *11* spacecraft were well equipped to provide a complementary investigation of magnetospheric science, although limited by the constraints on the trajectory (Figure 27.3). A number of thorough reviews of the *Pioneer* data already exist in the literature (Fillius 1976, Simpson and McKibben 1976, Van Allen 1976, McDonald and Trainor 1976, Kennel and Coroniti 1979, Siscoe 1979). Highlights of the comprehensive *Pioneer* data and a summary of data from the *Galileo* probe are presented here, along with a discussion of how the data

Table 27.1. Summary of in situ measurements in the inner jovian radiation belts.

Instrument	Data	Measurement range	References
Pioneer 10/11			
Helium Vector Magnetometer	vector magnetic field		Smith *et al.* (1976)
Flux Gate Magnetometer	vector magnetic field		Acuna and Ness (1976a,b)
Plasma Analyzer	electrons and protons	0.1–4.8 KeV	Frank *et al.* (1976)
Geiger Tube Telescope	electrons	>0.06, 0.55, 5, 21, 31 MeV	Van Allen *et al.* (1974, 1975, 1976)
	protons	0.61–3.41 MeV	Baker and Van Allen (1977)
Trapped Radiation Detector	electrons	>0.16, .26, .46, 5, 8, 12, 35 MeV	Fillius and McIlwain (1974)
	protons	>80 MeV	Fillius *et al.* (1975), Fillius (1976)
Low Energy Telescope	protons	1.2–2.15, 14.8–21.2 MeV	Trainor *et al.* (1974, 1975) McDonald and Trainor (1976)
Electron Current Detector	electrons	>3.4 MeV	Simpson *et al.* (1974, 1975)
Fission cell	protons	>35 MeV	Simpson and McKibben (1976)
Galileo Probe			
Energetic Particle Instrument	electrons	>3.2, >8 MeV	Fischer *et al.* (1992, 1996)
	protons	42–131, 62–131, 62–92 MeV nuc^{-1}	Mihalov *et al.* (1998)
	alphas	62–136 MeV nuc^{-1}	
	heavy particles	^{12}C: 110–910 MeV	
		^{32}S: >210 MeV	
Lightning and Radio Emission	radio wave	100 Hz to 100 kHz	Lanzerotti *et al.* (1992, 1996)
Detector Instrument	spectral analyzer	3, 15, 90 kHz channels	
	magnetic field	perpendicular to spin axis	
Galileo Orbiter			
Plasma instrument	electrons	0.9 V to 52 kV	Frank *et al.* (1992)
	protons	0.9 V to 52 kV	
Heavy Element Monitor	heavy ions	6 to 200 MeV nuc^{-1}	Garrard *et al.* (1992)
Dust Detector	dust grains	10^{-19} to 10^{-9} kg	Grun *et al.* (1992)
Plasma Wave	electric fields	5 Hz to 5.6 MHz	Gurnett *et al.* (1992)
	magnetic fields	5 Hz to 160 kHz	
Magnetic Field	vector magnetic field		Kivelson *et al.* (1992)
Energetic Particle Detector	electrons	15 keV to >11 MeV	Williams *et al.* (1992)
	ions	20 keV to 55 MeV	
	heavy ions	10 keV nuc^{-1} to 15 MeV nuc^{-1}	

constrain theoretical models. Table 27.1 provides a complete list of the in situ instruments that have traversed the inner radiation belts. The *Galileo* orbiter obtained observations into 2.5 R_J during the Amalthea flyby in November 2002, and thus these instruments are provided for completeness. Only preliminary analyses of these data were available at the time of publication (see section 27.7).

27.3.1 *Pioneer* Results

The *Pioneer 10* trajectory (Figure 27.3) approached Jupiter in a plane inclined 13.8° to the equatorial plane, approaching from the southern hemisphere, passing through the planet's equator, and reaching a periapsis distance of 2.85 R_J before exiting in the northern hemisphere. *Pioneer 11* followed a highly inclined trajectory that passed into the heart of the inner radiation belt, reaching a periapsis radius of 1.6 R_J. The *Pioneer* particle detectors provided an important set of measurements of the energy spectra, angular distributions, and radial profile of energetic electrons and protons. Unfortunately, neither *Pioneer* spacecraft was equipped with an instrument to measure low energy plasma, a measurement that remains unavailable today, and is pertinent to the estimate of how important processes such as wave–particle interactions are in the inner region (see later discussion of *Galileo* orbiter results). Energetic particle fluxes at various energies measured along the *Pioneer 10* and *11* trajectories are shown in Figures 27.4 and 27.5 respectively. The general trend of increasing flux with decreasing L was assumed by the *Pioneer* investigators to be evidence that radial diffusion is the primary source of transport in the radiation belts. The results demonstrate a clear sweeping effect (absorption) by the Galilean satellites and Amalthea. The angular distribution of the trapped radiation is also affected by satellite sweeping (section 27.2). Particles that mirror close to the equator can escape absorption by passing above or below the satellite orbital plane (Fillius 1976), due to the tilted nature of Jupiter's magnetic equator relative to the rotational equator. The flux minima due to sweeping by Amalthea are most evident in the higher energy channels, whereas the inner minima noted as N2 and N3 were considered as evidence for a particle ring (Fillius 1976). Although Fillius reports that the reasons for the structure are a mystery, hints to the complexity of the jovian radiation belts are evident in the data. In attempting to explain the signatures of absorption, Acuna and Ness (1976) noted the possibility of an inner satellite in addition to a particle ring. We now know that Jupiter's radiation belts contain both, rings and

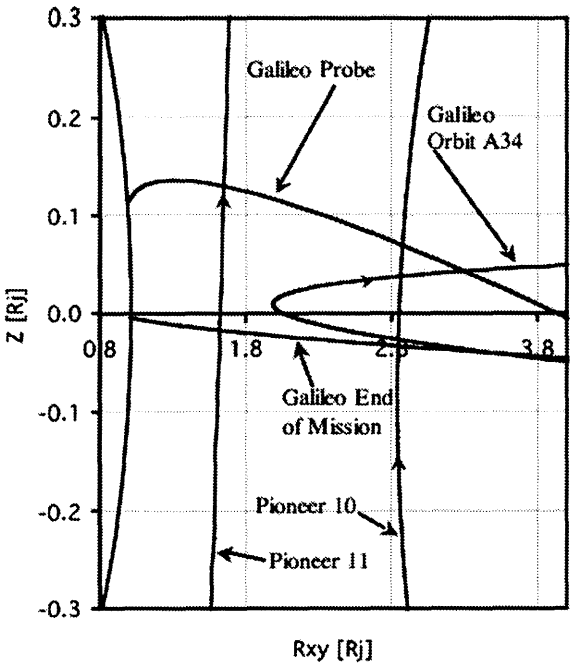

Figure 27.3. Trajectories of all spacecraft that have traversed the inner radiation belts: *Pioneer 10* and *11*, *Galileo* probe and orbiter. Models based on in situ data come from these locations only; in situ modeling at other locations must be interpolations or extrapolations, or, in some cases, extensions by using directional data and Liouville's theorem. Location along the time profiles of data presented in other figures can be inferred from features such as the peak at perijove and equatorial crossing, and the sweeping signatures of Jupiter's satellites and rings.

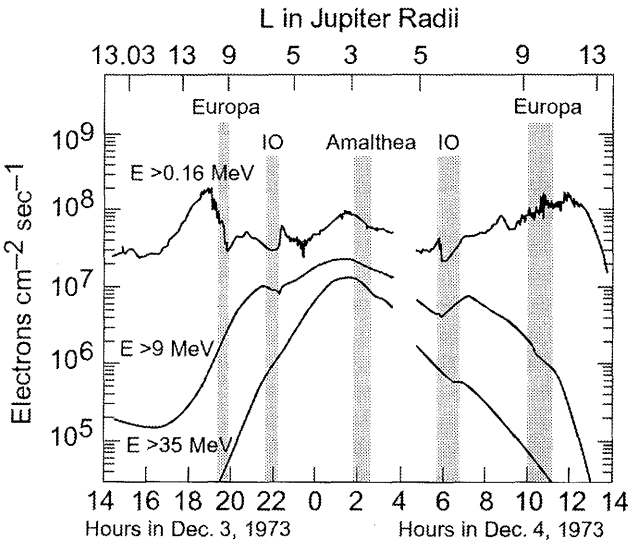

Figure 27.4. Trapped electron fluxes in Jupiter's inner radiation belts measured by the UCSD detector on *Pioneer 10*. Electron fluxes with $E > 0.16$ MeV, $E > 9$ MeV, and $E > 35$ MeV plotted against time and L-shell. Regions of L-shells corresponding to satellite sweeping are shaded. Omni-directional electron fluxes resulting from the attempt at background subtraction. The non-relativistic component of the energy spectrum is a negligible source of synchrotron radiation, both because the fluxes are low, and because these energies are inefficient producers of radiation. From Fillius and McIlwain (1974).

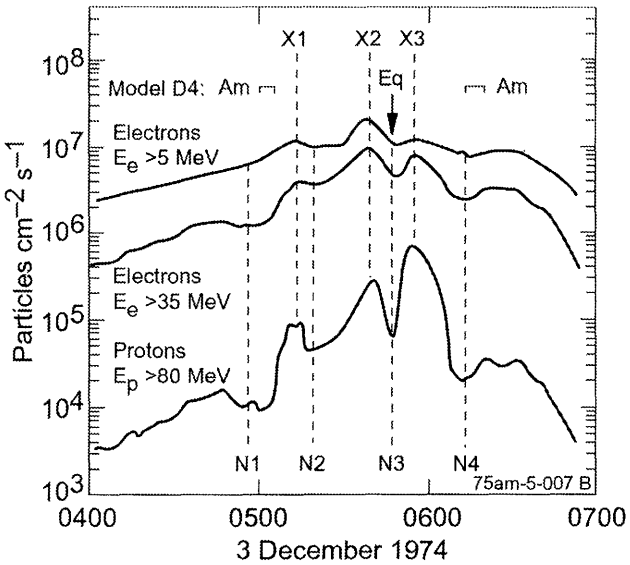

Figure 27.5. Electron and proton fluxes from UCSD instrument measured near the closest approach of *Pioneer 11* to Jupiter (1.6 R_J from the center of planet at 5h 23m). Peaks and minima are denoted by X and N, respectively. N1 and N4 are close to the orbit of Amalthea and thus were attributed to satellite sweeping. X1, X2 and X3 were located at 1.62 R_J, 1.66 R_J, and 1.82 R_J, respectively. N2 and N3 were located at 1.6 R_J and 1.74 R_J. At the time of *Pioneer*, the multiple peak structure was unexplained. Possible explanations included magnetic field anomalies, a dust ring, or some other possible cause. From Fillius (1976).

inner satellites that were unknown at the time of the *Pioneer* flybys.

Examples of the electron energy spectra measured from *Pioneer 10* at approximately 3 R_J and the pitch-angle distribution inferred from the latitudinal variation in particle flux measured on the two spacecraft (Baker and Van Allen 1976) are shown in Figure 27.6. Sentman and Van Allen (1976) also reported from analysis of *Pioneer 10* data that the inner core region at $R < 12$ R_J displayed a pancake angular distribution for all measured low energy electrons. The distributions were similar to those determined for higher energy electrons (>21 MeV) by the *Pioneer* investigators (Van Allen *et al.* 1974, Fillius and McIlwain 1974, and Simpson *et al.* 1974). The formation of pancake distributions in the inner magnetosphere is consistent with any inward radial transport mechanism. Kennel and Coroniti (1979) noted that the electron energy spectral hardening at lower L could also be a consequence of inward radial diffusion and weak synchrotron energy losses outside of $L = 3$. They further speculated that if the spectrum continued to harden to $L = 2$, it would approach the E^{-1} spectrum required to be consistent with the relatively flat decimetric frequency spectrum (as required by optically thin synchrotron emission theory).

27.3.2 Results from the *Galileo* Probe

The *Galileo* probe carried two instruments to measure energetic particles and radio and plasma wave activity in the inner radiation belts during the approach phase of the mission. Spot samples of data were recorded at approximately 5, 4 and 3 R_J, followed by a more continuous series of mea-

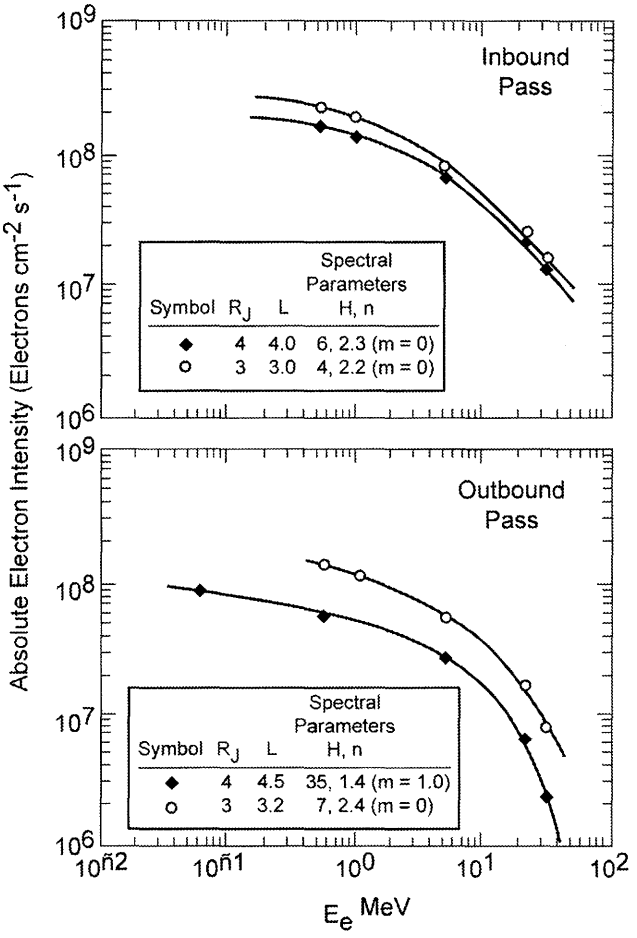

Figure 27.6. High energy electron energy spectra near $L = 3$ and 4 from *Pioneer 10*. Measured integral intensities are connected by smooth curves. The hardening of the spectrum at these low L-shells is consistent with inward radial diffusion and weak synchrotron energy losses outside of $L=3$. H and n are fitting parameters to the spectrum for the form $dJ/dE = kE-1.5(1+E/H)-n$ where J is the omni-directional intensity in cm^{-2} s^{-1} and E is the kinetic energy in MeV. The L-shell parameters are based on centered tilted dipole calculations. From Baker and Van Allen (1976).

surements (12 intervals) from 2.4 R_J to 1.25 R_J. The probe trajectory (see Figure 27.3) provided the first in situ radial profile through the equatorial region of the inner radiation belts. Results from the energetic particle instrument (EPI) are shown in Figure 27.7. The fluxes of energetic electrons and protons exhibit a general increase with decreasing radial distance, reaching a peak near the orbit of Amalthea. The fluxes then decrease near 2 R_J followed by a secondary inner peak near 1.5 R_J, consistent with the *Pioneer* multiple peak data described above. The EPI data indicate that the absorption feature (interpreted from *Pioneer* data analysis as due to satellite absorption) continues throughout the inner radiation belts to the vicinity of the main inner peak at ~1.5 R_J (this radial distance roughly corresponds to the equatorial peak region of the observed synchrotron emission). The reported peaks in He and heavy particles near 1.5 R_J are a factor of 10 greater than the minima within the main ring, presumably related to absorption by ring material. Fischer

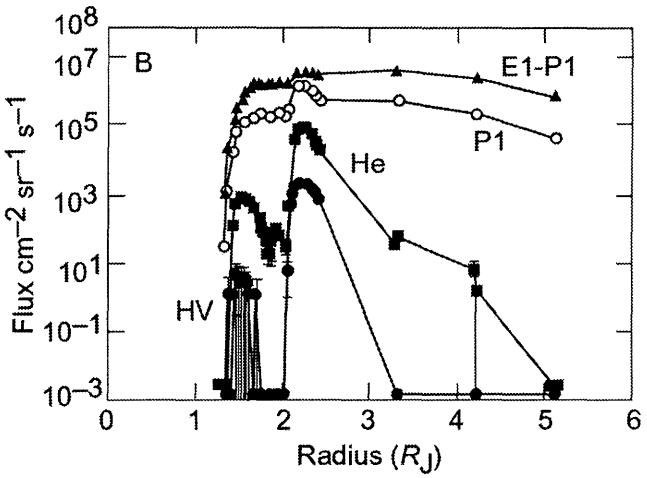

Figure 27.7. Data from *Galileo* probe EPI instrument. High energy particle observations in four species–energy channels are shown corresponding to E1 (e − 3.2 MeV, p + 42 MeV), P1 (e − 66 MeV, p + 42–131 MeV), He (e − 450 MeV, He 62–136 MeV per nucleon), HV (C 110–168 MeV per nucleon, S 210 MeV per nucleon). In this figure, E1–P1 represents spin-averaged electron intensities. The E1 channel has a lower limit of 3.2 MeV for electrons, and the subtraction of P1 removes proton background. Further details are provided by Fischer *et al.* (1996).

et al. (1996) speculate that the ion peaks at 1.5 R_J may originate from spallation of ring material by trapped protons and cosmic rays or cosmic ray sputtering of He from Jupiter's upper atmosphere.

Mihalov *et al.* (2000) have made a direct comparison between the probe and *Pioneer* electron data and also provide new measurements of electron pitch-angle distributions from the EPI instrument. Assuming power-law energy distributions, they conclude that the probe flux measurements are within a factor of three of similar energy channels from *Pioneer*. (For comparison, the synchrotron emission intensity levels at the time of the *Galileo* probe measurements were about 25% higher than during the *Pioneer* flybys (Klein *et al.* 2001).)

Figure 27.8 shows the values of power-law exponents for energetic electrons from the *Galileo* probe data. A spectral softening with decreasing pitch angle was reported for all locations. The energy spectrum for locally mirroring electrons appeared harder than corresponding locations reported for *Pioneer* by Van Allen (1976). The probe data also showed a gradual softening in the spectrum inside 2 R_J and a dramatic softening of the energy spectrum inside 1.5 R_J. Mihalov *et al.* (1998) associated these phenomena with energy loss in the atmosphere, although an alternate explanation could be extremely strong synchrotron radiation losses close to the planet due to the rapid increase in magnetic field magnitude.

27.4 SYNCHROTRON EMISSION OBSERVATIONS

Jovian radio emissions provide an important probe of the inner region of the radiation belts. Jupiter's decametric radio emission was used to initially define Jupiter's rotation

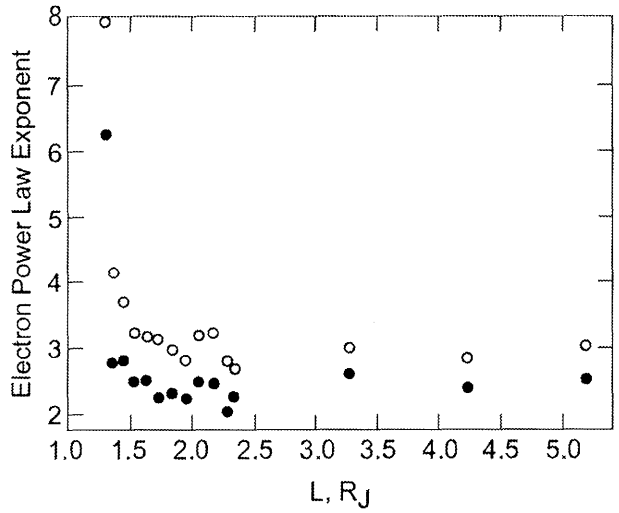

Figure 27.8. Values of power-law exponents for energetic electrons as determined from *Galileo* probe measurements. The solid symbols are for locally mirroring electrons, and the hollow symbols for the minimum pitch angle observed at each location. Note the spectra are consistently softer for the smaller pitch angles. From Mihalov *et al.* (2000).

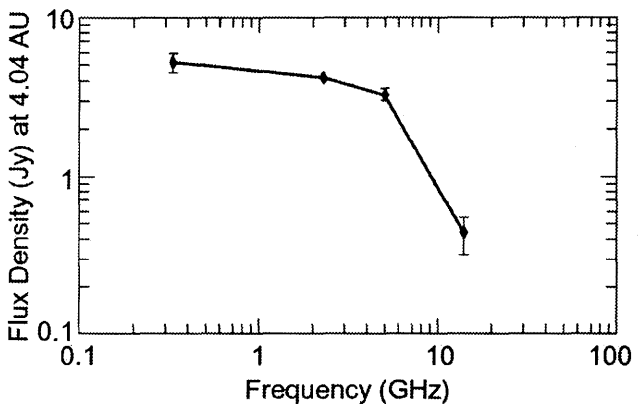

Figure 27.9. Jupiter's non-thermal radio spectrum. The observed flux density of Jupiter's synchrotron emission observed with *Cassini* (13.8 GHz) is plotted alongside simultaneous measurements obtained using the DSN (2.3 GHz) and the VLA (0.333 GHz). Previous measurements at 6 cm (5 GHz) are shown for completeness. All measurements are from January 2001 except for the 6-cm data from 1994. Error bars on the data are indicative of the preliminary nature of the results. From Bolton *et al.* (2002).

period (Higgins *et al.* 1997). Analysis of synchrotron emission in the decimeter band provided the basic structure of Jupiter's magnetic field as a tilted dipole, filled with trapped energetic electrons confined primarily to the magnetic equator. The properties of the non-thermal emission that led to these early conclusions were:

- The emission is continuous both in time and spectrally.
- The emission is distributed spatially, approximately four jovian radii east–west and two radii north–south.
- The emission is linearly polarized approximately 20–25% at wavelengths of 6–20 cm.

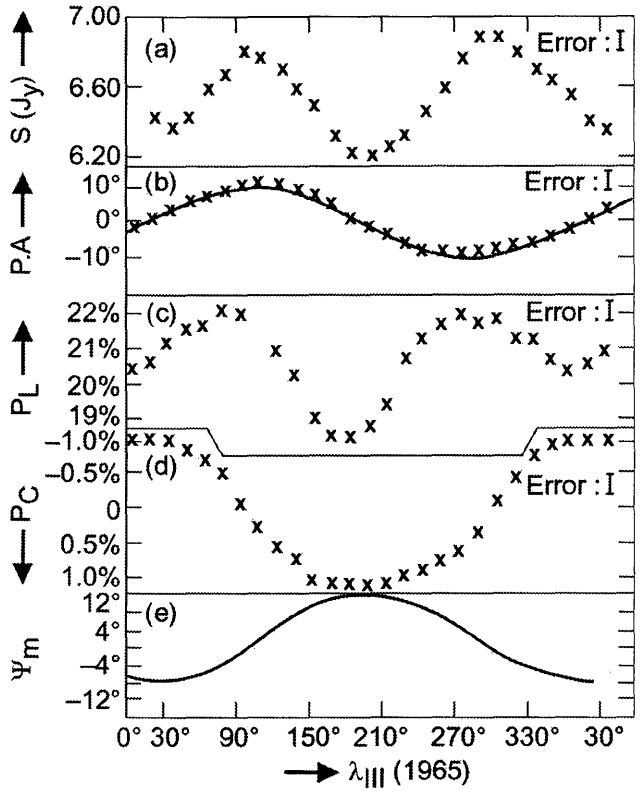

Figure 27.10. Various parameters of the integrated radiation of Jupiter at 21 cm wavelength as a function of System III longitude. Top panel to bottom: Total integrated flux density, position angle of the electric vector measured eastward from north in the sky, degree of linear polarization, degree of circular polarization, and magnetic latitude of the Earth with respect to Jupiter. From Carr, Desch and Alexander (1983).

- There is a weak circularly polarized component (~1%) that oscillates with Jupiter's rotation period (~10 hours).
- The total flux density varies with Jupiter's rotation, varying approximately 10%, with two peaks and valleys every 10 hours.

Because the theory of synchrotron emission is well understood, observations of the synchrotron component of Jupiter's radio emission are useful for improving our knowledge of the radiation belts within a few jovian radii. In order to more fully understand how synchrotron emission observations are used, and to appreciate the natural limitations associated with interpretation of the observations, we will briefly review some of the basic physics of radiation by high energy electrons in a magnetic field. More detailed treatments of synchrotron radiation are given by, e.g., Chang (1962), Chang and Davis (1962), Thorne (1965), Legg and Westfold (1968), and Carr, Desch and Alexander (1983). A single electron of charge e and mass m_e, given an initial velocity perpendicular to a uniform magnetic field, B, will revolve in a near circular path around the field line. The orbit radius will slowly increase due to the loss of energy from radiation. In a non-relativistic case, the radiation is emitted in the form of a monochromatic Hertzian dipole source with a frequency identical to that of the electron's revolution. This type of emission is cyclotron emission and the frequency is

the electron cyclotron frequency, or sometimes referred to as the gyrofrequency. If the perpendicular velocity of the electron relative to the magnetic field is relativistic, the radiation will be preferentially emitted (beamed) in the direction of the velocity vector (Jackson 1975). The beaming cone becomes narrower as the electron energy is increased with most of the radiation being beamed within a cone having a half-width (in radians) given by $1/2\gamma = (1/2)(1-\nu^2/c^2)^{1/2}$, where ν is the perpendicular velocity of the electron, and c is the speed of light. For a 20 MeV electron, the half-power beam full width is approximately 2.8 degrees. The polarization of the emission is linear when the observer's line of sight is perpendicular to **B**. A line of sight parallel to **B** will receive circularly polarized emission, right hand if **B** points toward the observer, and left hand if **B** points away from the observer.

In most cases, the velocity of the electron contains components both parallel and perpendicular to **B**, and the true path is helical rather than circular. For an electron of pitch angle α, the emission is confined to the surface of a thin cone with half-width $1/2\gamma$ and opening angle 2α. An observer in the path of the beam sees a broad spectrum consisting of a large number of harmonics of $f_c/\sin^2\alpha$, where f_c is the relativistic electron gyrofrequency. The emitted spectrum peaks at a frequency of $0.29\nu_c$ falling off rapidly at frequencies greater than the critical frequency $\nu_c = 16.08\ E^2 B \sin\alpha$, where E is the electron energy in MeV, B is the magnetic field in gauss, and ν_c is in MHz. The total power radiated by a single electron is given (in watts) by $P = 6 \times 10^{-22} E^2 B^2 \sin^2\alpha$. The observed emission from Jupiter effectively becomes a continuum due to the physical broadening from the full spatial distribution of emitting electrons in both energy and pitch angle. A 20 MeV electron with pitch angle 90° gyrating in a magnetic field of 1.0 gauss will radiate peak emission at 2 GHz (15 cm).

Observations of Jupiter synchrotron emission have proven to be valuable in constraining models for the electron distributions in the jovian radiation belts. Below we provide a brief explanation of each of the key measurement parameters associated with synchrotron emission observations and describe their relevance to models of Jupiter's electron radiation belts.

27.4.1 Flux Density

Total flux density of emission can be measured accurately using a radio telescope that does not resolve Jupiter or the radiation belts. The integrated flux density represents emission from electrons throughout the radiation belts and also includes thermal emission from Jupiter's atmosphere, which must be removed using a combination of techniques based on atmospheric models, drift scans, polarization and maps. The total flux density is usually normalized to a standard distance (typically 4.04 AU) for comparison with observations at different epochs and at different frequencies. The total flux density measurements provide spectral and time variability information on the synchrotron emission. The flux density has been continuously monitored at 13 cm since 1971 (Klein *et al.* 2001).

27.4.2 Spectrum

Determining the spectrum associated with synchrotron emission from trapped radiation belt electrons requires accurate separation of the thermal and non-thermal components of the radiation, which becomes increasingly more difficult at frequencies above 6 GHz, where the thermal emission is dominant. An example of the synchrotron spectrum from Jupiter is shown in Figure 27.9 (Bolton *et al.* 2002). The low frequency portion of the spectrum was obtained from Earth-based radio observations at wavelengths where thermal emission can easily be removed. The measurement at 13.8 GHz was obtained by mapping jovian radio emission with the *Cassini* radar/radiometer while en route to Saturn. Because the radiated power from relativistic electrons scales in proportion to E^2B^2, while the emitted frequencies scale as E^2B, the emission spectrum provides constraints on the energy distribution of the radiating electrons. The time variability of the spectrum is not sufficiently well measured to provide critical information for understanding the particle source and loss processes.

27.4.3 Beaming curve

The tilt (and non-dipolar components) of Jupiter's magnetic field, the anisotropic distribution of the relativistic electrons, and the narrow angle beaming of the synchrotron emission all combine to produce a ten-hour modulation in Jupiter's total flux density as Jupiter rotates (Figure 27.10). This periodic variation is referred to as the jovian beaming curve and is most accurately determined by total flux density measurements. The variation with central meridian longitude (CML, the jovian longitude facing the observer) shows two peaks corresponding to times when the observer's line of sight is tangent to Jupiter's magnetic equatorial plane. The characteristics of the beaming curve vary with D_E (declination of Earth as seen from Jupiter) and are time variable (Klein *et al.* 1989). The beaming curve is dominated by the emission from electrons in a pancake distribution near 1.4 R_J, and has been used to provide constraints on the pitch-angle distribution of the radiating electrons (Roberts 1976).

27.4.4 Polarization

Polarization information can be obtained from either single dish antennae or interferometric observations. The polarization can be broken down into linear (P_L) and circular (P_C) components. Figure 27.10 shows the variation of the P_L and P_C over one jovian rotation at a frequency of 1.4 GHz. Typically values for P_L and P_C are 0.25 and 0.01 respectively but vary with Jupiter's rotation. Measurements of the linear polarization provide constraints on the tilt of Jupiter's magnetic dipole (equivalent) and have potential to yield a great deal of information on the structure of the magnetic field and pitch-angle distribution of the electrons. Because the degree of linear polarization varies greatly over the spatial region of emission, interferometric maps are required to separate parameters. Since the electron energy spectrum varies spatially over the emission region, the average degree of linear polarization can also be expected to vary with frequency. This may be particularly important at very high frequencies where the emission originates from very high

Figure 27.11. VLA maps of Jupiter's synchrotron emission observed at 21 cm wavelength (1.4 GHz) in May 1997 when D_E = 0. Three orientations are shown corresponding to approximately 40, 180 and 280 degrees CML. The spatial resolution is approximately 0.25 R_J. Each image is averaged over approximately 40 degrees in longitude. The tilt of Jupiter magnetic equator and the two distinct emission regions (high latitude lobes and equatorial peaks) are clearly visible. Magnetic field lines corresponding to L = 1.5, 2.0, 2.5, 3.0 and 3.5 based on the VIP4 model are shown for reference. Note the high latitude lobe emission is associated with L = 2.5 while the equatorial peak emission is closer to L = 1.5. Thermal emission from the atmosphere has been subtracted. Courtesy of Bolton. At the time of going to press a colour version of this figure was available for download from http://www.cambridge.org/9780521035453.

energy electrons (or from regions of very strong magnetic field magnitude). The polarization characteristics above 5 GHz are currently undetermined (although data obtained recently with *Cassini* at 13.8 GHz is expected to yield an accurate estimate of the polarization at this frequency).

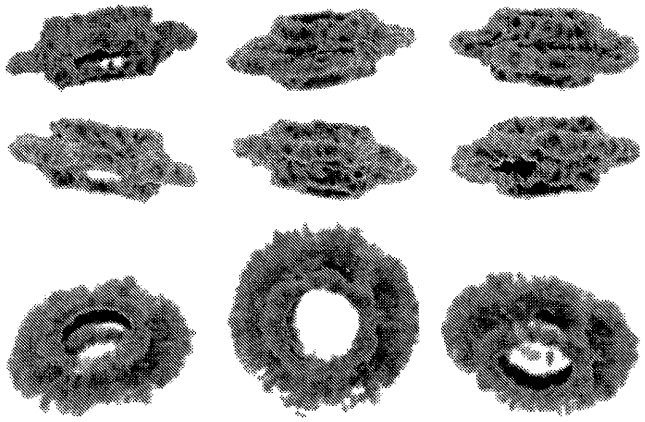

Figure 27.12. Three-dimensional reconstructions of Jupiter's radiation belts based on synchrotron emission observations at 13 cm wavelength. Maps are derived from 10 days of observing. Jupiter's thermal emission has been subtracted prior to the reconstruction. The warping of Jupiter's magnetic equator and two distinct emission regions (associated with the high latitude lobes and equatorial peaks) are clearly evident in the reconstructions. From Sault *et al.* (1997b).

27.4.5 Interferometric maps

Interferometric maps using multiple radio telescopes provide detailed information on the spatial distribution of the emission, which in turn provides constraints on the pitch-angle distribution and radial flux profile of the emitting electrons. The spatial distribution of the synchrotron emission obtained with the VLA at 1.4 GHz is shown in Figure 27.11. Compact peaks in the radiation occur near the magnetic equator at $L = 1.5$ and at high latitude near $L = 2.4$. A broad more diffuse region of emission extends in the magnetic equatorial plane outward from $L = 1.5$ to approximately $L = 4$, with somewhat less emission at higher latitudes. The emission varies considerably when viewed from different jovian longitudes with emission effectively disappearing from the equatorial region on one side or the other of the planet due to the multi-pole characteristic of Jupiter's magnetic field inside of $L = 2$ (see Figure 27.11 middle panel corresponding to 180° CML). This variation over Jupiter's rotation is further evidence of the narrow pancake distribution of energetic electrons and the narrow beaming of the synchrotron emission itself.

Sault *et al.* (1997a) used tomographic principles to develop three-dimensional reconstructions of Jupiter's synchrotron radiation from interferometric observations. The three-dimensional reconstructions provide a number of new insights into the structure of Jupiter's inner radiation belts, although the technique requires an assumption that the emission is isotropic, when in fact the emission is narrowly beamed (see Section 27.4). Sault *et al.* suggest the resulting errors from ignoring the beaming are not significant compared with errors due to the limited Fourier coverage and other deconvolution errors. The technique further assumes there is no intrinsic change to the source during the observation. If data are averaged over timescales of days to weeks, short-term variations could therefore cause additional errors.

The 3-D reconstructions show the warping of the magnetic equator (Figure 27.12) as well as revealing that the

latitude and radial distance of peak emissivity lies on the magnetic equator on a surface of constant L (Leblanc *et al.* 1997b, Dulk *et al.* 1997a). Using the 3-D reconstructions, Dulk *et al.* (1997a) showed that the polarized brightness maxima at high latitudes originate from electrons near $L = 2.37$ with an average pitch angle of $\sim 27°$. The proximity of the electrons to Amalthea led Dulk *et al.* (1997a) to propose that the satellite may play a role in pitch angle scattering electrons to produce the high latitude lobe emission. Dulk *et al.* (1999a) examined equatorial brightness distribution as a function of CML. They developed an explanation based on the magnetic declination at Jupiter's magnetic equator (the angle between jovigraphic north and jovimagnetic north). This simple concept provided the basis for comparing models of Jupiter's magnetic field in the inner region of Jupiter's radiation belts. Dulk *et al.* (1999b) showed that the VIP4 magnetic field model (Connerney *et al.* 1998) was not completely consistent with synchrotron emission observations, suggesting the potential for constraining future magnetic field models using synchrotron emission observations.

27.5 STRUCTURE AND VARIABILITY OF THE INNER RADIATION BELTS

A combination of the radio telescope and in situ investigations over the last few decades has yielded knowledge of Jupiter's radiation belts which provides a basic picture of a population of relativistic electrons trapped in a slightly offset, near dipolar and tilted magnetic field. The electrons can be coarsely described by a two-component pitch-angle distribution, consisting of a highly anisotropic pancake component and a more isotropic distribution that interacts with Jupiter's atmosphere through loss cone processes. The two-component model first introduced by Roberts (1976) has been used as the basis of many subsequent synchrotron radiation models (e.g., de Pater 1981, Levin *et al.* 2001).

Both long and short term variations in the synchrotron emission (Figure 27.13) have been reported (Klein *et al.* 2001, Bolton *et al.* 2002). Considerable effort has been made to identify processes responsible for the variations, although it should be noted that the magnitude of the variations is relatively small (less than a factor of 2), especially when compared to uncertainties in the observed in situ energy spectra. Nevertheless, the strength of Jupiter's magnetic field in this region and the energies of the electrons responsible for the synchrotron emission create a challenge to theorists attempting to explain even 10–20% variability in the synchrotron zone. No viable process has been put forward for local acceleration in the inner jovian radiation belts, although wave-induced local stochastic acceleration is thought to be potentially important in the Earth's radiation belts, particularly in regions of low plasma density (Summers *et al.* 1998, Horne *et al.* 2003). The mechanism of cross L diffusion is a relatively slow process in the strong magnetic field region close to the planet. A correlation between the long-term variations of the synchrotron emission flux density and the solar wind has been reported by Bolton *et al.* (1989) with a lag time of 1–2 years, consistent with the diffusion coefficients suggested by Brice and Ioannidis (1970). Miyoshi *et al.* (1999) have reported that some short-term variation of synchrotron radiation is correlated with solar F10.7 flux

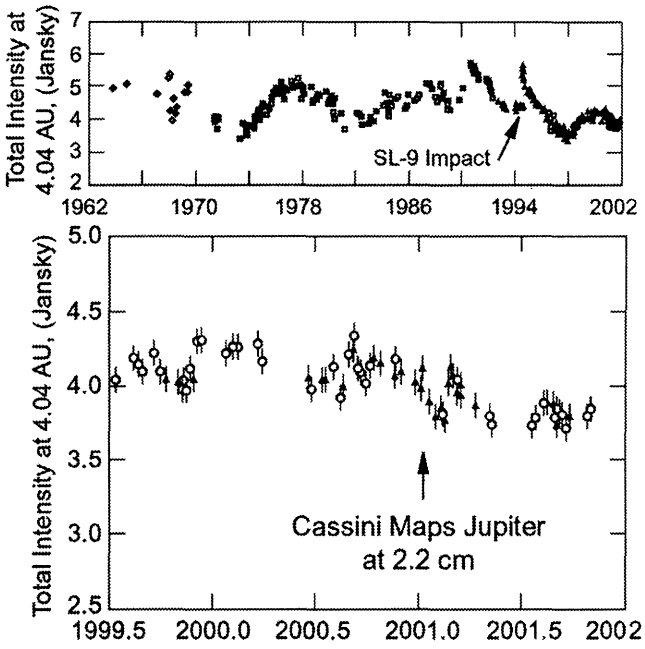

Figure 27.13. Total flux density measurements of Jupiter's synchrotron emission as function of time as observed at 13 cm wavelength. Both short term (days to weeks) and long term (weeks to months) variations are evident in the data sets. The time period of the SL-9 impacts into Jupiter (1994) and the *Cassini* flyby of Jupiter (2001) are shown for reference. Courtesy of Klein.

enhancements and suggested that this may be due to enhanced radial diffusion due to atmospheric heating associated with an increase in solar UV/EUV flux.

From the remote radio studies, and in situ particle measurements, and analogy with the terrestrial radiation belt theory, a basic picture of the jovian radiation belts has emerged. The general pancake distributions of the energetic particles in the system are well ordered and assumed to be a result of inward radial diffusion with conservation of the first and second adiabatic invariants, μ and J and from the inevitable loss to the atmosphere, satellites and ring particles. The distribution of the particles in the corotating frame of reference is relatively time-stationary. The characteristic timescale for radial diffusion and synchrotron radiation is approximately a year for relativistic electrons in the heart of the synchrotron zone. Due to the greater complexity of Jupiter's system (rings, dust, and satellites) and the magnitude of the jovian magnetic field ($\sim$10 times stronger than Earth's), Jupiter's radiation belts are more energetic, more complex and have a much greater variety of processes governing them. High-order terms in the magnetic field, together with the relativistic beaming characteristics of synchrotron emission, and the relative pancake pitch-angle distribution of the electrons produce significant asymmetries in the observed synchrotron radiation as a function of System III longitude.

The question of short term time variability in the synchrotron emission was most directly witnessed with the recent collision of Comet Shoemaker–Levy 9 into Jupiter's atmosphere. The synchrotron emission increased significantly directly after the first impact. While the details of the

processes responsible for the observed changes have thus far eluded all modeling efforts, the major effect on the radiation belts has been understood to be related to the latitude and longitude of the impact site. Analysis by Bolton and Thorne (1995) showed the impacts occurred on field lines connecting Jupiter's atmosphere to the synchrotron emission region ($1.4 < L < 2.5$). Dulk *et al.* (1997b) further showed that the effects were localized to the magnetosphere at the longitudes of the impact sites, and that an increase in emission remained at the same longitudes for up to a week, even though the relativistic electrons responsible for the increased emission have drift periods of a few days. Observations of the beaming curve before and after the impacts indicated the impacts caused a general "flattening" (Bolton *et al.* 1995, Klein *et al.* 1995). Various authors describe a variety of mechanisms to accomplish the observed changes to the emission properties. Early concepts focused on three primary mechanisms: enhanced radial diffusion (Ip 1995), shock induced electron energization (Bolton and Thorne 1995, Brecht *et al.* 1995, Dulk *et al.* 1995), and impact generated waves inducing electron pitch angle scattering (Bolton and Thorne 1995). No single mechanism or model has been shown to be fully consistent with all observations. A detailed review of the observations and physical processes associated with the magnetospheric effects from the Shoemaker–Levy 9 impacts is given by (Leblanc *et al.* 1997a, Bolton 1997). Further details of effects from the impacts are discussed in Chapter 8.

27.6 MODEL RESULTS

Prior to the *Pioneer* flybys, quantitative theoretical models of various aspects of Jupiter's magnetosphere were developed both to assess the potential hazard to the *Pioneer* spacecraft and to provide a basis for analysis of the spacecraft and remote radio observations (Coroniti 1974, Kennel and Coroniti 1975). The *Voyager 1* and *2* spacecraft did not pass directly into the inner radiation belts, but the information obtained on the middle magnetosphere led to a more reliable model, which was used to make predictions of the environment around Jupiter and to assist in interpreting the wealth of data from synchrotron observations.

Divine and Garrett (1983) developed the first quantitative model of Jupiter's radiation belts, by combining the in situ *Pioneer* and *Voyager* data with the remote observations of the synchrotron emission. Limited data from the single inclined trajectories of the *Pioneer* spacecraft did not provide detailed constraints on the particle distributions inside of 5 R_J. However, the Divine–Garrett model did match the *Pioneer* data remarkably well along the trajectory paths of the spacecraft. Unfortunately, the model parameters, which controlled the electron pitch angle and latitude distributions inside the *Pioneer 10* perijove ($L < 2.85$), were not strongly constrained by the *Pioneer 11* data. The relatively poor match to the synchrotron emission observations (compared to the match to the *Pioneer* data) indicated that more observations were needed (Divine and Garrett 1983). Despite the shortcomings mentioned above, the Divine–Garrett model made valuable contributions to our overall understanding of the jovian environment, enabling accurate estimates of the radiation shielding requirements for both *Galileo* and *Ulysses* spacecraft. Data from *Galileo* orbiter obtained at radial distances greater than 6 R_J matched predictions by the model with reasonable accuracy.

De Pater (1981) developed a model capable of simulating synchrotron emission observations from a particle distribution in a multi-polar magnetic field. The model specified the particle distribution $j(E, \alpha)$ at a particular location, on a specified L-shell, and estimated the L-dependence of Jupiter's electron distribution from an analytical model for radial diffusion (Goertz *et al.* 1979). The effect on the particle distributions due to synchrotron radiation loss and absorption by satellites, Jupiter's ring, and the jovian atmosphere were also included. The satellites and ring produced distinct changes in $j(E, \alpha)$ at the L-shells involved. The model assumed that particles drift around Jupiter along contours of constant equatorial magnetic field strength. The electron distribution was constrained using in situ *Pioneer* data (Van Allen *et al.* 1975). Subsequently de Pater and Goertz (1990) developed a numerical code for particle diffusion to examine the effects on the synchrotron radiation resulting from changes in the particle population and/or diffusion properties. After the report that the high latitude lobe emission was connected to L-shells near Amalthea (Dulk *et al.* 1997a), de Pater reported to fit the synchrotron observations to their model, they required an electron distribution with a step function increase in the number of small pitch angle electrons at Amalthea's orbit (de Pater *et al.* 1997). De Pater *et al.* proposed that electrons were pitch-angle scattered in "whistler wings" produced by the satellites' interaction with Jupiter's magnetosphere. No physical mechanism for the scattering was ever identified. The role of Amalthea in maintaining the high latitude relativistic electron population remains controversial, since data from the recent *Galileo* flyby does not indicate an increase in whistler wave activity or an extended interaction region associated with the moon (see section 27.7). Other models (Santos-Costa *et al.* 2001) only suggest electrons are lost by satellite sweeping at Amalthea.

Levin *et al.* (2001) have developed a computer code to simulate the synchrotron emission from an adjustable but empirical model for relativistic electrons trapped in Jupiter's magnetic field. The code generates the four Stokes parameters of the synchrotron emission for various electron distributions and magnetic field models. The model includes a true volume integral in three-dimensional space and takes into account the relativistic beaming effects of synchrotron emission. The resulting two-dimensional Stokes parameter maps can be compared directly with ground-based radio observations. Using the VIP4 magnetic field model (Connerney *et al.* 1998), electron distributions are tailored to fit synchrotron emission observations. The gross features of data from both VLA and single-dish observations are fit by a longitudinally symmetric particle distribution. Levin *et al.* (2001) were able to accurately model the beaming curve, including the variation with D_E (declination of the Earth), using a symmetric particle population. This confirmed that high order terms in the magnetic field are primarily responsible for the beaming curve and observed rotational asymmetries. Levin *et al.* further reported that the beaming curve is a sensitive measure of the electron pitch angle distributions, noting that with more isotropic distributions, the beaming curve flattens. Previous work by Dulk *et al.* (1997a)

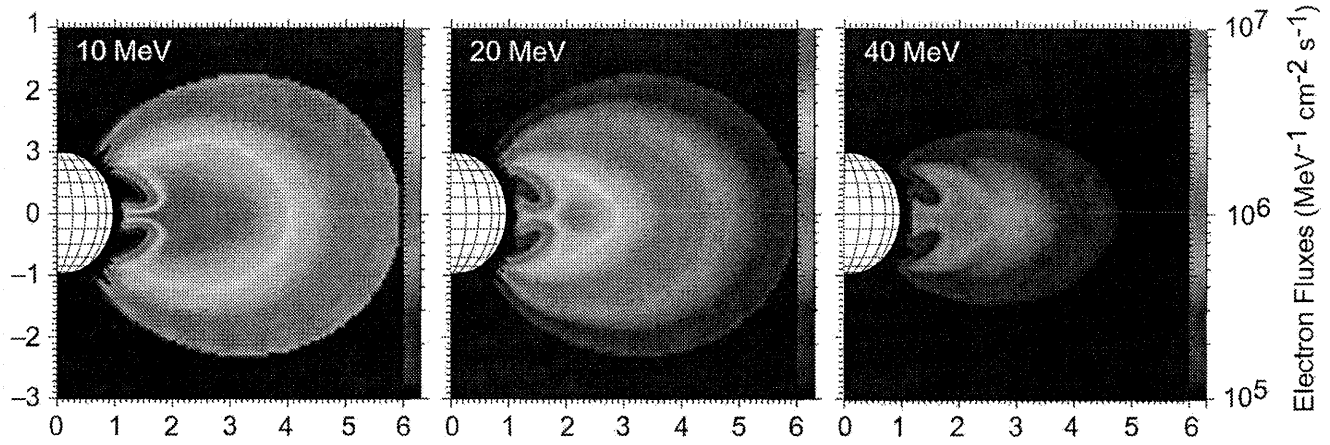

Figure 27.14. Omni-directional differential electron fluxes in a meridian plane for three energies. Electron spatial distribution is a function of radial distance, kinetic energy and latitude. Energy spectrum decreases with energy and particles are confined at the magnetic equator and close the planet. High latitudes particles are strongly affected by ring interactions, synchrotron process and moons effect. From Santos-Costa (2001).

suggested the symmetric particle distribution was responsible for the rotational asymmetries and D_E variations, and de Pater *et al.* (1997) was also able to approximately fit a model to the beaming curve with a longitudinally symmetric particle population at one $D_E(-3°)$. The work by Levin *et al.* and others clearly demonstrated that a "hot spot" in the particle distribution was not required to model the rotational asymmetries as earlier suggested (Branson 1968, de Pater 1981). Levin *et al.*'s model was later used to compare the Divine–Garrett model with synchrotron emission observations. They found the relative intensities of the equatorial and high latitude peak emission were not very well simulated using the Divine–Garrett particle distribution functions (at $L < 3$) (Bolton *et al.* 2001). The distributions were corrected, but a new Divine–Garrett model was not yet published as of the date of this book (Garrett, personal communication).

A three-dimensional transport code (Salammbo), initially built to model Earth's radiation belts (Beutier and Boscher 1995), has recently been adapted to model Jupiter (Santos-Costa *et al.* 2001). The model calculates particle distribution functions as a function of the three adiabatic invariants by solving the Fokker–Planck diffusion equation, using diffusion coefficients to account for the processes that violate each of the three invariants. The principal advantage of the Salammbo code over other diffusion models is the ability to investigate processes affecting the particles at locations away from the equator, and thus obtain the 3-D structure of the radiation belts. When all the relevant processes (section 27. 2) are properly accounted for, the model results show good agreement with the limited data available from *Pioneer* observations (Santos-Costa and Bourdarie 2001). The model fluxes have also been used to generate a simulated pattern of synchrotron radiation (Santos-Costa *et al.* 2001), which contains most of the prominent features seen in VLA maps.

Recent model runs with the Salammbo code (Figure 27.14) use *Galileo* data to define the external boundary near $L = 6$. Radial diffusion, Coulomb interactions, synchrotron radiation loss, sweeping effects of the jovian moons, and interaction with dust particles, are modeled as free parameters. In addition to the selective sweeping by satellites, based on the particle's pitch angle and energy, an important new aspect of the Salammbo modeling is the treatment of high energy particle interactions with dust particles. Early models treated the ring system as an absorber (de Pater 1981, de Pater and Goertz 1990, Hood 1993, Miyoshi *et al.* 1999). The more sophisticated treatment by Santos-Costa (2001) recognizes that electrons both lose energy and experience a deflection. Absorption occurs only when the electron energy is below the threshold required to pass through the dust, with the threshold energy dependent on the size and mass of the dust particle. During ring crossings, the electrons lose energy through inelastic collisions and Bremsstrahlung radiation. Pitch angle diffusion also occurs via deflection when an electron passes completely through the dust. Santos-Costa (2001) report strong ring effects in the densest regions (1.25 R_J to 1.81 R_J) with strongest effects restricted to particles with pitch angle near 70 degrees. The effect is diminished in the region outside of 1.81 R_J, with almost negligible effects outside of 2.6 R_J. They suggest that energy degradation of electrons in the ring near Amalthea leads to a decrease in the particle's perpendicular (to B) energy component and therefore a decrease in the particle's pitch angle. Synchrotron radiation losses can also significantly modify the pitch-angle distribution because the electron predominantly radiates energy from the perpendicular component (Santos-Costa *et al.* 2001). Furthermore, at $L < 1.4$ the synchrotron energy losses becomes so severe that few high energy electrons are able to penetrate closer to the planet, forming a sharp inner edge to the synchrotron emission. Motivated by the longitudinally asymmetric gap between the emission peaks and the atmosphere of Jupiter, Wang *et al.* (2002) explored the possibility that the source of the steep fall-off in the synchrotron emission at $L < 1.4$ was related to atmospheric losses. They found that the observed peak emission is significantly further from the planet than predicted by the outer bound of electron loss, and deduced that other processes (such as radiative losses) must be important in dictating the inner edge of the radiation belts.

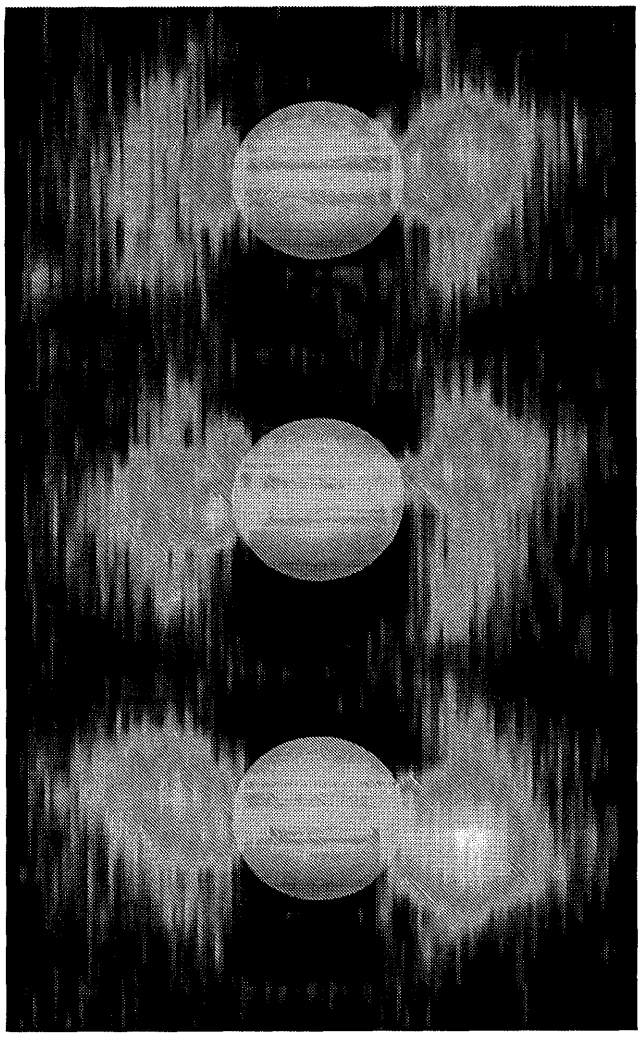

Figure 27.15. Color maps of Jupiter's synchrotron emission at 2.2 cm wavelength (13.8 GHz) obtained with the *Cassini* Radar instrument during the Jupiter flyby in 2001. Three orientations are shown corresponding to approximately 33, 177 and 285 degrees CML. The electrons responsible for synchrotron emission at 13.8 GHz are substantially higher energy than the electrons responsible for the emission at 1.4 GHz (see Figure 27.11). Map resolution is approximately 0.3 R_J. A visible image constructed from Hubble Space Telescope and *Voyager* data is shown superimposed for context. Thermal emission from the atmosphere has been subtracted. Courtesy of Bolton. At the time of going to press a colour version of this figure was available for download from http://www.cambridge.org/9780521035453.

27.7 RECENT DEVELOPMENTS

Recent observations by *Cassini* during the Jupiter flyby en route to Saturn provided the first accurate measure and map of Jupiter's synchrotron emission at frequencies above ~8 GHz. The measurements provide an important additional constraint on models of the inner radiation belts. Because synchrotron emission has a well defined spectrum that falls off rapidly at frequencies above ν_c, determining Jupiter's radio spectrum at all frequencies can be used to constrain the electron energy distributions. Knowledge of the electron energy spectrum as a function of L and pitch angle remains a fundamental issue in developing models consistent with both the in situ data and the synchrotron emission. The *Cassini*

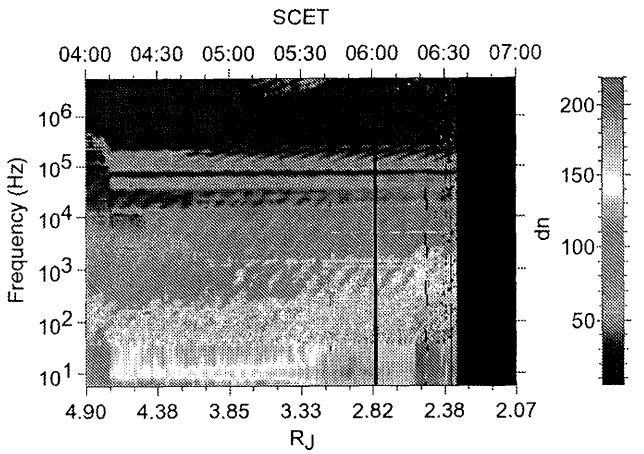

Figure 27.16. Plasma wave intensities as a function of time as measured by the Plasma Wave Spectrometer on the *Galileo* orbiter during the flyby of Amalthea (November 2002). Note the increase in wave intensity at the radial distances of Thebe and Amalthea. No direct signature of the moon Amalthea is evident. Increased wave intensity at the orbital radius of both moons could be associated with changes in the gossamer rings. Courtesy of D. Gurnett, University of Iowa.

observations extended the known spectrum out to 13.8 GHz, representing electrons above 50 MeV near the peak emission regions. Although models have yet to exploit this new information, the extended radio spectrum combined with the spatial information from the maps shown in Figure 27.9 provide key information on the energy distributions as a function of L and pitch angle. Note the relative intensities between the equatorial and high latitude peaks in the maps at 13.8 GHz (Figure 27.15) compared to the 1.4 GHz maps shown in Figure 27.11. Unfortunately, the *Cassini* observations had poorer resolution than VLA observations at the lower frequencies and a direct comparison is difficult. However, a decrease in the relative intensities of the high latitude peaks at 13.8 GHz is apparent in the separate polarization maps (see Bolton *et al.* 2002). If correct, this would imply a softer electron energy spectrum at small pitch angles, consistent with *Galileo* probe results (Mihalov *et al.* 2000).

On November 5, 2002, the *Galileo* orbiter approached Jupiter to within 2 R_J of planet center, passing through the gossamer ring region and providing a close flyby of the satellite Amalthea. Plasma wave data from this period is shown in Figure 27.16. A marked increase in the plasma wave activity, at frequencies below the proton gyrofrequency, is evident radially inward of the orbital radius of Thebe (~3.1 R_J). Such wave activity increases again radially inward of the orbital radius of Amalthea (~2.4 R_J). As discussed in Chapter 11, the gossamer ring properties are known to evolve at the satellite's orbital radius and thus an increase in the particle–dust interaction could be responsible for the increased wave activity. Alternatively, the increased wave activity could also be due to an unknown spacecraft interaction with the increased ring material. The spacecraft came within 165 km of Amalthea, within the Hill sphere of this moon, although no obvious plasma wave signature of an interaction region was observed. The spacecraft was equipped with a suite of magnetospheric instruments (see Table 27.1), however, no other data were available in time

to be included in this manuscript. In particular, the plasma density remains undetermined, which could provide important constraints on wave modes present and hence the potential for wave–particle interaction. In September 2003, the spacecraft will again pass through the inner radiation belts en route to Jupiter's atmosphere. We can only hope that the spacecraft systems will hold out through this harsh region and provide us with yet one more in situ set of observations of Jupiter's inner radiation belts. The potential for breakthrough science is substantial, as the combination of plasma wave, plasma, energetic particles, and dust measurements through the main ring region could provide the most important data set of Jupiter inner radiation belts since *Pioneer 10* and *11* first encountered the giant planet.

27.8 OUTSTANDING QUESTIONS AND FUTURE DIRECTIONS

At present no model exists that is consistent with both the in situ data and remote synchrotron emission features. The Divine–Garrett model fits the in situ data quite well, with deviations falling easily within what might be expected from dynamics and time variability. However, this model provides a relatively poor fit to the spatial distribution of the synchrotron emission, the beaming curve variation over Jupiter's rotation, and both the overall intensity and spectrum of the radio emission. The Salammbo transport code extends the Divine–Garrett capabilities by providing a reasonable fit to the spatial distribution of the synchrotron emission, and has demonstrated promise to accurately model the beaming curve, although currently this is not as good as the synchrotron simulation models of de Pater *et al.* (1997), Levin *et al.* (2001), and Bolton *et al.* (2001). A key constraint that has eluded all models thus far is the overall intensity and spectrum of the synchrotron emission. Models that fit these two parameters fail to provide a reasonable fit to the in situ data of either *Pioneer* or *Galileo*. In almost all of the models the energy dependence of Jupiter's electron flux is modeled by a double power law (e.g., Van Allen 1976). With a specified electron energy distribution, the models described above can be used to derive a radio spectrum, which can be compared to observations. Current attempts at this have not been successful. However, the new *Cassini* data may provide the basis for significant progress in the near future. While both radio spectra and the spatial brightness distribution of the emission are affected by the choice of parameters in the electron spectra, the radial diffusion parameters and (energy dependent) particle losses will be affected as well. Furthermore, the system is time variable, so a solution at one particular time may not necessarily apply to the steady state.

Our understanding of the inner magnetosphere of Jupiter has improved substantially since Chris Goertz in 1990 elucidated the key questions about the origin of Jupiter's inner radiation belts based on *Pioneer* and *Voyager* data. However, as our understanding of the belts has evolved, important new questions have arisen such as:

- Are particles significantly energized by processes other than radial diffusion?
- What are the causes of the long and short term variations observed in the synchrotron emission?
- What is the energy distribution of the relativistic electrons and is there a maximum energy?
- What maintains the electron pitch-angle distribution?
- What is the source of the "double" radiation belt observed in the *Galileo* probe data?
- What are the roles of dust, ring particle and wave interactions in developing the semi-stable particle distribution functions that are observed in the inner jovian radiation belts?

Even after more than 25 years of study, the inner jovian radiation belts remain largely unexplored except for the limited measurements made by the *Galileo* probe (primarily the EPI instrument), the single passes of *Pioneer 10* and *11*, and the remote synchrotron emission observations. There remains a great deal of mystery surrounding the inner radiation belts. The EPI instrument indicated a softening of the energetic electron (>21 MeV) energy spectrum with decreasing pitch angle. This was very coarsely measured by EPI, and it would be important to confirm and extend the measurements to know if this trend extends to lower energies (> 1 MeV). The basic electron energy spectrum remains one of the least understood issues in the inner radiation belts; knowledge of this would discriminate among current models of the radiation belts and provide a basis for testing the observed synchrotron emission radio spectrum. There is limited knowledge of the protons and ions in the region, and one of the most important outstanding questions that remains is the low energy plasma density. This is key to identifying the wave modes that might be present. There is an obvious evolution of wave activity at the orbital radius of Thebe and again at Amalthea. Whether these waves could resonate with relativistic electrons to explain the maintenance of the isotropic electron distribution inside of 2.5 R_J is an important issue that the *Galileo* orbiter may be able to address in the near future. The interaction of ring material and dust with the high-energy radiation is another important aspect that is not well constrained. Lastly, the multiple peaks observed in the high-energy particle flux by both *Pioneer* and *Galileo* probe remain another unresolved issue. Some of the flux minima can be explained by satellite absorption as suggested by a number of *Pioneer* investigators. However, why there are secondary peaks in electrons, helium and heavy particle rates near $L = 1.5$ is still a mystery.

In the last few years a number of new Jupiter missions capable of addressing many of the outstanding questions raised above have been proposed. While none of the missions has yet been selected for funding, awareness of the jovian radiation belts has steadily increased, due to the recent progress reported here and the scientific interest in orbital missions to further explore Jupiter, its auroral zone, Europa and the other Galilean satellites, as described in the recent NRC decadal reports.

Acknowledgements. The authors thank D. Santos-Costa and S. Levin for valuable contributions. A portion of this research was carried out at the Jet Propulsion Laboratory, California Institute of Technology, under a contract with the National Aeronautics and Space Administration and at UCLA under NASA grant NAG5-11216.

REFERENCES

Abel, B. and R. M. Thorne, Electron scattering loss in Earth's inner magnetosphere: 1. Dominant physical processes, *J. Geophys. Res.* **103**, 2385–2396, 1998.

Abel, B. and R. M. Thorne, Relativistic charged particle precipitation into Jupiter's sub-auroral atmosphere, *Icarus* **166**, 311, 2003.

Acuna, M. H. and N. F. Ness, The main magnetic field of Jupiter, *J. Geophys. Res.* **81**, 2917–2922, 1976.

Baker, D. N. and J. A. van Allen, Energetic electrons in the jovian magnetosphere, *J. Geophys. Res.* **81**, 617–632, 1976.

Beutier, T. and D. Boscher, A three-dimensional analysis of the electron radiation belt by the Salammbo code, *J. Geophys. Res.* **100**, 14 853–14 862, 1995.

Bird, M. K., O. Funke, J. Neidhofer, and I. de Pater, Multifrequency radio observations of Jupiter at Effelsberg during the SL9 impact, *Icarus* **121**, 450–456, 1996.

Birmingham, T., W. Hess, T. Northrup, R. Baxter, and J. Lujko, The electric diffusion coefficient in Jupiter's magnetosphere, *J. Geophys. Res.* **79**, 87, 1974.

Bolton, S. J., Interpretation of the observed changes in Jupiter's synchrotron radiation during and after the impacts from Comet Shoemaker–Levy 9, *Planet. Space Sci.* **45**, 1359–1370, 1997.

Bolton, S. J. and R. M. Thorne, Assessment of mechanisms for jovian synchrotron variability associated with Comet SL9, *Geophys. Res. Lett.* **22**, 1813, 1995.

Bolton, S. J., S. Gulkis, M. J. Klein, I. de Pater, and T. J. Thompson, Correlation studies between solar wind parameters and the decimetric radio emission from Jupiter, *J. Geophys. Res.* **94**, 121–128, 1989.

Bolton, S. J., R. S. Foster, and W. B. Waltman, Observations of Jupiter's synchrotron radiation at 18 cm during the Comet Shoemaker–Levy 9 impacts, *Geophys. Res. Lett.* **22**, 1801, 1995.

Bolton, S. J., S. M. Levin, S. L. Gulkis, M. J. Klein, R. J. Sault, B. Bhattacharya, R. M. Thorne, G. A. Dulk, and Y. Leblanc, Divine–Garrett model and jovian synchrotron emission, *Geophys. Res. Lett.* **28**, 907, 2001.

Bolton, S. J., M. Janssen, R. Thorne, S. Levin, M. Klein, S. Gulkis, T. Bastian, R. Sault, C. Elachi, M. Hofstadter, A. Bunker, G. Dulk, E. Gudim, G. Hamilton, W. T. K. Johnson, Y. Leblanc, O. Liepack, R. McLeod, J. Roller, L. Roth, and R. West, Ultra-relativistic electrons in Jupiter's radiation belts, *Nature* **415**, 987–991, 2002.

Branson, N. J. B. A., High resolution observations of the planet Jupiter, *MNRAS* **139**, 155, 1968.

Brautigam, D. H. and J. M. Albert, Radial diffusion analysis of outer radiation belt electrons during the October 9, 1990, magnetic storm, *J. Geophys. Res.* **105**, 291–310, 2000.

Brecht, S. H., M. Pesses, J. G. Lyon, N. T. Gladd, and S. W. McDonald, An explanation of synchrotron radiation enhancement following the impact of Shoemaker–Levy 9 with Jupiter, *Geophys. Res. Lett.* **22**, 1805, 1995.

Brice, N. M. and G. A. Ioannidis, The magnetospheres of Jupiter and Earth, *Icarus* **13**, 173, 1970.

Brice, N. M. and T. R. McDonough, Jupiter's radiation belts, *Icarus* **18**, 206–219, 1973.

Bunce, E. J. and S. W. H. Cowley, Divergence of the equatorial current in the dawn sector of Jupiter's magnetosphere: Analysis of *Pioneer* and *Voyager* magnetic field data, *Planet. Space Sci.* **49**, 1089–1113, 2001.

Burke, B. F. and K. L. Franklin, Observations of a variable radio source associated with the planet Jupiter, *J. Geophys. Res.* **60**, 213, 1955.

Carr, T. D., M. D. Desch, and J. K. Alexander, Phenomenology of magnetospheric radio emissions, in *Physics of the Jovian Magnetosphere*, A. J. Dessler (ed.), Cambridge University Press, pp. 226–284, 1983.

Chang, D. B. and L. J. Davis, Synchrotron radiation as the source of Jupiter's polarized decimeter radiation, *ApJ* **136**, 567, 1962.

Chang, D. B. J., Synchrotron radiation as the source of the polarized decimeter radiation from Jupiter., *AJ* **67**, 112, 1962.

Connerney, J. E. P., M. H. Acuña, N. F. Ness, and T. Satoh, New models of Jupiter's magnetic field constrained by the Io flux tube footprint, *J. Geophys. Res.* **103**, 11 929–11 940, 1998.

Cornwall, J. M., Scattering of energetic trapped electrons by very-low-frequency waves, *J. Geophys. Res.* **69**, 1251–1258, 1964.

Coroniti, F. V., Energetic electrons in Jupiter's magnetosphere, *ApJS* **27**, 261, 1974.

Coroniti, F. V., Denouement of jovian radiation belt theory, *Space Sci. Rev.* **17**, 837–856, 1975.

de Pater, I., A comparison of radio data and model calculations of Jupiter's synchrotron radition: 2. East-west asymmetry in the radiation belts as a functon of jovian longitude, *J. Geophys. Res.* **86**, 3423–3429, 1981.

de Pater, I. and C. K. Goertz, Radial diffusion models of energetic electrons and Jupiter's synchrotron radiation: I. Steady state solution, *J. Geophys. Res.* **95**, 39–50, 1990.

de Pater, I., M. Schulz, and S. H. Brecht, Synchrotron evidence for Amalthea's influence on Jupiter's electron radiation belt, *J. Geophys. Res.* **102**, 22 043–22 064, 1997.

Divine, N. and H. B. Garrett, Charged particle distributions in Jupiter's magnetosphere, *J. Geophys. Res.* **88**, 6889–6903, 1983.

Drake, F. D. and S. Hvatum, Non-thermal microwave radiation from Jupiter, *AJ* **64**, 329, 1959.

Dulk, G. A., Y. Leblanc, and R. W. Hunstead, Flux and images of Jupiter at 13, 22, and 36 cm before, during, and after SL9 impacts, *Geophys. Res. Lett.* **22**, 1789, 1995.

Dulk, G. A., Y. Leblanc, R. J. Sault, H. P. Ladreiter, and J. E. P. Connerney, The radiation belts of Jupiter at 13 and 22cm: II. The asymmetries and the magnetic field, *A&A* **319**, 282–289, 1997a.

Dulk, G. A., R. J. Sault, and Y. Leblanc, Jupiter's radiation belts: At the time of comet SL-9 and a year later, *Planet. Space Sci.* **45**, 1231–1236, 1997b.

Dulk, G. A., Y. Leblanc, R. J. Sault, and S. J. Bolton, Jupiter's magnetic field as revealed by the synchrotron radiation belts: II. Change of the 2-D brightness distribution with D. E, *A&A* **347**, 1039–1045, 1999a.

Dulk, G. A., Y. Leblanc, R. J. Sault, S. J. Bolton, J. H. Waite, and J. E. P. Connerney, Jupiter's magnetic field as revealed by the synchrotron radiation belts: I. Comparison of a 3-D reconstruction with models of the field, *A&A* **347**, 1029–1038, 1999b.

Dungey, J. W., Loss of Van Allen electrons due to whistlers, *Planet. Space Sci.* **11**, 591–596, 1963.

Field, G. B., The source of radiation from Jupiter at decimeter wavelengths, *J. Geophys. Res.* **64**, 1169, 1959.

Fillius, R. W. and C. E. McIlwain, Measurements of the jovian radiation belts, *J. Geophys. Res.* **79**, 3589, 1974.

Fillius, W., The trapped radiation belts of Jupiter, in *Jupiter*, T. Gehrels (ed), University of Arizona Press, pp. 896–927, 1976.

Fischer, H. M., E. Pehlke, G. Wibberbez, L. J. Lanzerotti, and J. D. Mihalov, High-energy charged particles in the innermost jovian magnetosphere, *Science* **272**, 856–858, 1996.

Goertz, C. K., Plasma in the jovian magnetosphere, *J. Geophys. Res.* **81**, 2007–2014, 1976.

Goertz, C. K., J. A. van Allen, and M. F. Thomsen, Further observational support for the lossy radial diffusion model of the inner jovian magnetosphere, *J. Geophys. Res.* **84**, 87–92, 1979.

Higgins, C. A., T. D. Carr, F. Reyes, W. B. Greenman, and G. R. Lebo, A redefinition of Jupiter's rotation period, *J. Geophys. Res.* **102**, 22 033–22 041, 1997.

Hill, T. W., Interchange stability of a rapidly rotating magnetosphere, *Planet. Space Sci.* **24**, 1151–1154, 1976.

Hood, L. L., Energetic particle absorption by atmosphereless satellites and rings, *Adv. Space Res.* **13**, 10, 1993.

Horne, R. B., S. A. Glauert, and R. M. Thorne, Resonant diffusion of radiation belt electrons by whistler-mode chorus, *Geophys. Res. Lett.* **30**, 46–1, 2003.

Ip, W.-H., Time variations of the jovian synchrotron radiation following the collisional impacts of Comet Shoemaker–Levy 9: 2. Flux enhancement induced by neutral atmospheric turbulence, *Planet. Space Sci.* **43**, 221–223, 1995.

Jackson, J. D., *Classical Electrodynamics*, Wiley, 1975.

Kennel, C. F. and F. V. Coroniti, Is Jupiter's magnetosphere like a pulsar's or Earth's?, in *The Magnetospheres of the Earth and Jupiter*, p. 451, 1975.

Kennel, C. F. and F. V. Coroniti, Jupiter's magnetosphere and radiation belts, in *Solar System Plasma Physics, Volume 2: Magnetospheres*, pp. 105–181, 1979.

Klein, M. J., T. J. Thompson, and S. Bolton, Systematic observations and correlation studies of variations in the synchrotron radio emission from Jupiter, in *Time-Variable Phenomena in the Jovian System*, M. J. S. Belton, R. A. West, J. Rahe (eds), NASA, pp. 151–155, 1989.

Klein, M. J., S. Gulkis, and S. J. Bolton, Changes in Jupiter's 13-cm synchrotron radio emission following the impact of Comet Shoemaker–Levy 9, *Geophys. Res. Lett.* **22**, 1797, 1995.

Klein, M. J., S. J. Bolton, S. Gulkis, M. A. Janssen, S. J. Levin, J. P. Roller, and R. K. McLeod, *Cassini*-Jupiter microwave observing campaign: DSN and GAVRT observations of jovian synchrotron radio emission, in *Planetary Radio Emissions V*, p. 221, 2001.

Krimigis, S. M., J. F. Carbary, E. P. Keath, C. O. Bostrom, W. I. Axford, G. Gloeckler, L. J. Lanzerotti, and T. P. Armstrong, Characteristics of hot plasma in the jovian magnetosphere: Results from the *Voyager* spacecraft, *J. Geophys. Res.* **86**, 8227–8257, 1981.

Leblanc, Y., R. J. Sault, and G. A. Dulk, Synthesis of magnetospheric radio emissions during and after the Jupiter/SL-9 collision, *Planet. Space Sci.* **45**, 1213–1221, 1997.

Legg, M. P. C. and K. C. Westfold, Elliptic polarization of synchrotron radiation, *ApJ* **154**, 499, 1968.

Levin, S. M., S. J. Bolton, S. L. Gulkis, M. J. Klein, B. Bhattacharya, and R. M. Thorne, Modeling Jupiter's synchrotron radiation, *Geophys. Res. Lett.* **28**, 903, 2001.

Lyons, L. R. and R. M. Thorne, Equillibrium structure of radiation belt electrons, *J. Geophys. Res.* **78**, 2142–2149, 1973.

Lyons, L. R., R. M. Thorne, and C. F. Kennel, Pitch angle diffusion of radiation belt electrons within the plasmasphere, *J. Geophys. Res.* **77**, 3455, 1972.

Mauk, B. H., D. J. Williams, R. W. McEntire, K. K. Khurana, and J. G. Roederer, Storm-like dynamics of Jupiter's inner and middle magnetosphere, *J. Geophys. Res.* **104**, 22 759–22 778, 1999.

McClain, E. F. and R. M. Sloanaker, Preliminary observations at 10 cm wavelength using the NRL 84 foot radio telescope, in *Proceedings IAU Symposium No. 9-URSI, No.1*, R. N. Bracewell, ed., vol. 61, Stanford University Press, 1959.

McDonald, F. B. and J. H. Trainor, Observations of energetic jovian electrons and protons, in *Jupiter*, T. Gehrels (ed), University of Arizona Press, pp. 961–987, 1976.

Mihalov, J. D., H. M. Fischer, E. Pehlke, and L. J. Lanzerotti, Energetic trapped electron measurements from the *Galileo* Jupiter probe, *Geophys. Res. Lett.* **27**, 2445–2448, 2000.

Miyoshi, Y., H. Misawa, A. Morioka, T. Kondo, Y. Koyama, and J. Nakajima, Observation of short-term variation of Jupiter's synchrotron radiation, *Geophys. Res. Lett.* **26**, 9, 1999.

Mogro-Campero, A., R. W. Fillius, and C. F. McIlwain, *Space Research*, vol. XV, chap. Electrons and protons in Jupiter's radiation belts, Berlin Acadamie Verlag, 1975.

Ockert-Bell, M. E., J. A. Burns, I. J. Daubar, P. C. Thomas, J. Veverka, M. J. S. Belton, and K. P. Klaasen, The structure of Jupiter's ring system as revealed by the *Galileo* imaging experiment, *Icarus* **138**, 188–213, 1999.

Radhakrishnan, V. and J. A. Roberts, Polarization and angular extent of the 960-Mc/sec radiation from Jupiter, *Phys. Rev. Lett.* **4**, 493–494, 1960.

Roberts, J. A., The pitch angles of electrons in Jupiter's radiation belt, *Proc. Astron. Soc. Australia* **3**, 53–55, 1976.

Santos-Costa, D., *Modélisation des Ceintures de Readiation d'Électrons de Jupiter Internes à Io*, Ph.D. thesis, 2001.

Santos-Costa, D. and S. A. Bourdarie, Modeling the inner jovian electron radiation belt including non-equatorial particles, *Planet. Space Sci.* **49**, 303–312, 2001.

Santos-Costa, D., R. Sault, S. Bourdarie, D. Boscher, S. Bolton, R. Thorne, Y. Leblanc, G. Dulk, S. Levin, and S. Gulkis, Synchrotron emission images from three-dimensional modeling of the jovian electron radiation belts, *Adv. Space Res.* **28**, 915–918, 2001.

Sault, R. J., Y. Leblanc, and G. A. Dulk, Localized brightenings in Jupiter's radiation belts resulting from Comet SL9 impacts, *Geophys. Res. Lett.* **24**, 2395, 1997a.

Sault, R. J., T. Oosterloo, G. A. Dulk, and Y. Leblanc, The first three-dimensional reconstruction of a celestial object at radio wavelengths: Jupiter's radiation belts, *A&A* **324**, 1190–1196, 1997b.

Schulz, M. and L. J. Lanzerotti, *Particle Diffusion in the Radiation Belts*, Springer, 1974.

Sentman, D. D. and J. A. van Allen, Angular distributions of electrons of energy greater than 0.06 MeV in the jovian magnetosphere, *J. Geophys. Res.* **81**, 1350–1360, 1976.

Showalter, M. R., J. A. Burns, J. N. Cuzzi, and J. B. Pollack, Jupiter's ring system: New results on structure and particle properties, *Icarus* **69**, 458–498, 1987.

Simpson, J. A. and R. B. McKibben, Dynamics of the jovian magnetosphere and energetic particle radiation, in *Jupiter*, T. Gehrels (ed), University of Arizona Press, pp. 738–766, 1976.

Simpson, J. A., D. Hamilton, G. Lentz, R. B. McKibben, A. Mogro-Campero, M. Perkins, K. R. Pyle, A. J. Tuzzolino, and J. J. O'Gallagher, Protons and electrons in Jupiter's magnetic field: Results from the University of Chicago experiment on *Pioneer 10*, *Science* **183**, 306–309, 1974.

Siscoe, G. L., *Towards a Comparative Theory of Magnetospheres*, pp. 319–402, North-Holland, 1979.

Sloanaker, R. M., Apparent temperature of Jupiter at a wave length of 10 cm, *AJ* **64**, 346–346, 1959.

Summers, D., R. M. Thorne, and F. Xiao, Relativistic theory of wave–particle resonant diffusion with application to electron acceleration in the magnetosphere, *J. Geophys. Res.* **103**, 20 487–20 500, 1998.

Thorne, K. S., Dependence of Jupiter's decimeter radiation on electron distribution in van Allen belts, *J. Res. Nat. Bureau Standards Section D-radio science* **D69**, 1557, 1965.

Thorne, R. M., Microscopic plasma processes in the jovian magnetosphere, in *Physics of the Jovian Magnetosphere*, A. J. Dessler (ed.), Cambridge University Press, pp. 454–488, 1983.

Thorne, R. M., D. J. Williams, L. D. Zhang, and S. Stone, Energetic electron butterfly distributions near Io, *J. Geophys. Res.* **104**, 14 755–14 766, 1999.

van Allen, J. A., The geomagnetically trapped corpuscular radiation, *J. Geophys. Res.* **64**, 1683, 1959.

van Allen, J. A., High-energy particles in the jovian magnetosphere, in *Jupiter*, T. Gehrels (ed), University of Arizona Press, pp. 928–960, 1976.

van Allen, J. A., D. N. Baker, B. A. Randall, M. F. Thomsen, D. D. Sentman, and H. R. Flindt, Energetic electrons in the magnetosphere of Jupiter, *Science* **183**, 309–311, 1974.

van Allen, J. A., B. A. Randall, D. N. Baker, C. K. Goertz, D. D. Sentman, M. F. Thomsen, and H. R. Flindt, *Pioneer 11* observations of energetic particles in the jovian magnetosphere, *Science* **188**, 459–462, 1975.

Walt, M. and W. MacDonald, The influence of the Earth's atmosphere on geomagnetically trapped particles, *Rev. Geophys.* **2**, 543–577, 1964.

Wang, K., S. J. Bolton, S. M. Gulkis, and S. M. Levin, Atmospheric loss of energetic electrons in the jovian synchrotron zone, *Planet. Space Sci.* **50**, 277–285, 2002.

Williams, D. J., R. M. Thorne, and B. Mauk, Energetic electron beams and trapped electrons at Io, *J. Geophys. Res.* **104**, 14 739–14 754, 1999.

Ye, G. and T. P. Armstrong, Electron distributions in the inner jovian magnetosphere: *Voyager 1* observations, *J. Geophys. Res.* **98**, 21 253, 1993.